



LAWRENCE  
LIVERMORE  
NATIONAL  
LABORATORY

# Ceramic Coatings for Corrosion Resistant Nuclear Waste Container Evaluated in Simulated Ground Water at 90°C

J. J. Haslam, J. C. Farmer

April 1, 2004

Metallurgical and Materials Transactions

## **Disclaimer**

---

This document was prepared as an account of work sponsored by an agency of the United States Government. Neither the United States Government nor the University of California nor any of their employees, makes any warranty, express or implied, or assumes any legal liability or responsibility for the accuracy, completeness, or usefulness of any information, apparatus, product, or process disclosed, or represents that its use would not infringe privately owned rights. Reference herein to any specific commercial product, process, or service by trade name, trademark, manufacturer, or otherwise, does not necessarily constitute or imply its endorsement, recommendation, or favoring by the United States Government or the University of California. The views and opinions of authors expressed herein do not necessarily state or reflect those of the United States Government or the University of California, and shall not be used for advertising or product endorsement purposes.

# **Ceramic Coatings for Corrosion Resistant Nuclear Waste Container Evaluated in Simulated Ground Water at 90°C**

**Dr. Jeffery J. Haslam and Dr. Joseph C. Farmer**  
**Lawrence Livermore National Laboratory**  
**7000 East Avenue, L-353**  
**Livermore, California 94550**  
**Email: haslam2@llnl.gov**

This work was performed under the auspices of the U.S. Department of Energy by University of California, Lawrence Livermore National Laboratory under Contract W-7405-Eng-48.

## **Abstract**

Ceramic materials have been considered as corrosion resistant coatings for nuclear waste containers. Their suitability can be derived from the fully oxidized state for selected metal oxides. Several types of ceramic coatings applied to plain carbon steel substrates by thermal spray techniques have been exposed to 90°C simulated ground water for nearly 6 years. In some cases no apparent macroscopic damage such as coating spallation was observed in coatings. Thermal spray processes examined in this work included plasma spray, High Velocity Oxy Fuel (HVOF), and Detonation Gun. Some thermal spray coatings have demonstrated superior corrosion protection for the plain carbon steel substrate. In particular the HVOF and Detonation Gun thermal spray processes produced coatings with low connected porosity, which limited the growth rate of corrosion products. It was also demonstrated that these coatings resisted spallation of the coating even when an intentional flaw (which allowed for corrosion of the carbon steel substrate underneath the ceramic coating) was placed in the coating. A model for prediction of the corrosion protection provided by ceramic coatings is presented. The model includes the effect of the morphology and amount of the porosity within the thermal spray coating and provides a prediction of the exposure time needed to produce a crack in the ceramic coating.

## Introduction

The United States currently intends to provide a reliable storage of spent fuel rods from nuclear reactors and high level nuclear waste in a below ground repository for a period of time exceeding 10,000 years. While there are many facets of providing reliable protection of the waste material from causing adverse effects on the environment a particular challenge is corrosion of the waste package by aqueous environments in the proposed repository [1]. Under extreme conditions of high temperature oxidizing or acid environments it may be difficult to find metals that will protect against corrosion. Inorganic oxide materials (ceramic) may be the only materials that can provide sufficiently low dissolution rates of container materials under these conditions. Additionally, in some scenarios use of ceramic coatings on metallic substrates would provide significant cost savings to the waste package design and mitigate aggressive crevice corrosion conditions. In particular covalent oxide compounds in their highest normal oxidation states are unlikely to participate directly in electrochemical or galvanic corrosion mechanisms. It is helpful to consider that an inorganic oxide film is a relatively thick and fully oxidized version of the passivating films that generally are responsible for corrosion-resistance in many metals. It is expected that with the constituent elements in their fully oxidized state dissolution mechanisms are the only likely material loss process for covalent metal oxide compounds.

While there are several ways to produce ceramic coatings, for this application corrosion resistant coatings with a solid impervious coating of 0.015" (~380 $\mu$ m) or greater is desirable. Thermal spray processes potentially can provide an impervious coating of this thickness in an industrially amenable process. Plasma thermal spray technology uses a plasma to produce in the spray gun. Powder is fed into the plasma and accelerated by the expanding gas used to form the plasma. The heated molten particles hit the substrate and deform and cool to form a densified film. Other thermal spray technologies use a similar approach of heating and accelerating the particles to high velocity. High Velocity Oxy-Fuel (HVOF) and Detonation Gun spray processes generally can produce higher velocities to produce greater deformation of the particles when the particles hit the substrate. The porosity that remains in most thermal spray coatings is associated with the interfaces between the particles. In particular HVOF and Detonation Gun coatings have shown the possibility of water impervious inorganic coatings [2].

## Experimental

Samples of plain carbon steel (ANSI 1020) were coated with thermal spray techniques to produce ceramic coatings of various oxide ceramics. Oxide ceramics are selected with a preference for covalent compounds in their fully oxidized state. Alumina, Spinel ( $\text{MgAl}_2\text{O}_4$ ), and Alumina/Titania ( $\text{Al}_2\text{O}_3/\text{TiO}_2$ ) are some compositions that have been sprayed onto these substrates. Plasma spray, High Velocity Oxy-Fuel, and Detonation Gun thermal spray techniques have been used. Each technique has certain advantages.

Plasma spray utilizes the discharge of electricity through a plasma gas to create very high temperature zone within the spray gun. The powder is fed into this plasma and simultaneously heated and accelerated towards a substrate where the powder particles hit (“splat”) onto the substrate which cools the molten particles rapidly to form a solid coating. The high temperature in the plasma under proper conditions will usually melt ceramic particles. Propelling the particles towards the substrate at high velocity helps to deform the molten particles to form a coating that has a much higher density than random packing of the particles without the deformation. Both heating and velocity of the particles are important to producing strong dense coatings. Plasma spray does not always produce the highest particle velocity although it is often capable of very high temperatures. The substrate for the coating often functions as an effective heat sink to rapidly solidify the ceramic particles.

High Velocity Oxy-Fuel (HVOF) thermal spray is a slightly different type of coating process. In this case the gun functions as a supersonic combustion nozzle. Fuel and oxidizing gases are supplied to the combustion chamber along with the powder (usually the powder is delivered with a carrier gas) where the combustion produces supersonic flow through a nozzle within the gun. The powder is accelerated to relatively high velocities while being heated by the combustion process. Generally, much higher particle velocities can be obtained with HVOF thermal spray. Under the right operating conditions this leads to relatively higher density coatings. This is primarily attributed to the higher particle velocities, which produce greater deformation to aid in causing the particles to conform to both the substrate and coating particles already applied to the substrate. The plasma and HVOF thermal spray guns are illustrated in Figure 1.

Detonation Gun thermal spray uses a similar gun design to HVOF except that a supersonic nozzle is not present. The combustion process is pulsed by a spark ignition of the fuel and oxidizer. Even higher particle velocities are obtained using the Detonation Gun. The Detonation Gun designs have often included valves to cycle the flow of fuel and oxidizer to the combustion chamber; however, more recent designs have resulted in a valve-less Detonation Gun.

Table I shows a summary of coatings that were evaluated for corrosion resistance that are presented in this work. In these experiments, 1-inch (25.4 mm) diameter steel samples approximately 6 inches (150 mm) long were coated by thermal spray processes. The samples were weighed before placing them in the long-term corrosion tanks. The solutions for the tanks were prepared at 10X concentration of typical well water. The approximate composition of some species in the solution are shown in the Table II:

Table I. Performance of Thermal Spray Ceramic Coatings in Simulated 10X Concentrated Groundwater

Ceramic Type	Thermal Spray Process	Porosity (Volume %)	Coating Electrical Impedance	Corrosion Conditions	General Corrosion Observation	Corrosion at Intentional Notch
Al <sub>2</sub> O <sub>3</sub>	Plasma Spray	~20%	10 Ω at 10 Hz	90°C, 6 months, ~6 years	6 Mo. and ~6 yr.: Coating Blisters	6 Mo.: Coating spalls at notch
Al <sub>2</sub> O <sub>3</sub> /TiO <sub>2</sub>	HVOF	<2%	100 MΩ at 10 Hz	90°C, 6 months	6 Mo.: None	6 Mo.: No detectable corrosion at interface
Al <sub>2</sub> O <sub>3</sub> /TiO <sub>2</sub>	Detonation Gun	<2%		90°C, ~6 years	6 yr.: Negligible	~6yrs.: Small amount of corrosion at interface – attributed mostly to galvanic action

Table II. Concentration of Selected Ions (ppm) in the Corrosion Tank

Na <sup>+</sup>	SO <sub>4</sub> <sup>-2</sup>	Cl <sup>-</sup>	NO <sub>3</sub> <sup>-</sup>	HCO <sub>3</sub> <sup>-</sup>
460	180	74	64	700

For these experiments the bath was heated to 90°C and maintained with circulation in a sealed container. The samples were positioned so that half of the sample was above the water line. In some samples the specimens were cut with a diamond saw along the length of the sample to cut through the ceramic coating. The width of the notch was approximately 0.015” (~380 μm). The intent of the slot was to allow corrosion of the substrate below the ceramic coating and to examine the effects of the corrosion product upon the integrity of the thermal spray coating. The slot in this case simulates a large flaw in the coating.

Electrical impedance measurements were made on sections of the ceramic coated thermal spray samples. Measurements were recorded between 10 Hz and 10 kHz. Cross sections of the thermal spray coated samples were made by polishing sections through the slotted region of the sample. In some cases etching was used to help distinguish corrosion products from the metal substrate. The microstructures shown in this work are from the immersed portion of the samples.

## Results and Discussion

### A. Performance of Ceramic Coatings in Long-Term Corrosion Environment

The alumina plasma sprayed coating shown in the scanning electron micrograph in Figure 2 had a high amount of porosity approaching 20% by volume. The obvious interconnection of the porosity seen in the planar cross-section image leads to high permeability for the aqueous solution, which provides for relatively rapid oxygen

transport to the metal substrate. Oxygen transport is believed to be the rate limiting corrosion transport step in these coatings. It should also be noted that the porosity has a lamellar structure aligned perpendicular to the particle spray direction. This is a characteristic of thermal spray processes. Since the lamellar shape of the porosity is clearly observable, it is likely that the three dimensional shape of the porosity in the plasma sprayed alumina coating is extensive and probably amply interconnected. In the plasma sprayed alumina microstructure shown in Figure 2 the porosity is associated with incomplete fusing or adhesion of overlaying particle splats [3]. Impedance measurements at low frequency, which we associate with the diffusive process for transport of oxygen through the thermal spray coating, show low impedance. The low electrical impedance implies easy transport of the oxygen through the porosity in the plasma sprayed coating.

In contrast the cross-section of the HVOF sample shown in Figure 2 shows isolated porosity in the planar cross-section. In this case the overall porosity is much less, around 2% by volume. Obviously, it is possible that some connective channels may exist but they are not easily revealed in the cross-section suggesting that the capillary interconnections within the microstructure are less frequent and quite possibly rather tortuous. In the HVOF thermal spray sample, the low frequency impedance measurement shows a relatively high resistance compared to the plasma sprayed alumina ceramic coating. In fact the impedance at low frequencies is seven orders of magnitude greater in the HVOF sample. We conclude that this indicates the high resistance to diffusion of oxygen through the ceramic coating in the HVOF thermal spray coating. With regards to the processing, the high impedance at low frequency implies superior coating performance is obtained with the higher velocity thermal spray process. The lower porosity in the HVOF coating and a microstructure with reduced capillary size and/or more tortuous path provides a more resistive path for oxygen diffusion, which reduces the corrosion on the steel substrate.

The corrosion products from corrosion of the metal substrate for the plasma sprayed alumina and the HVOF alumina/titania are observed in optical micrographs in Figure 3. These micrographs show the samples after 6 months exposure in the 90°C concentrated well water solution. In the plasma sprayed alumina sufficient amounts of corrosion product have formed at the interface between the coating and the plain carbon steel substrate such that the alumina coating begins to lift off particularly near the intentional flaw (notch) in the coating. The intentional notch was cut through the ceramic coating prior to placement of the sample in the tank. In contrast no detectable corrosion product is observed at the metal ceramic interface near a similar intentional notch in the HVOF sample. The low permeability of the HVOF coating combined with a likely improvement in bond strength associated with less porosity at the interface lead to no detectable corrosion product in these micrographs.

Macroscopic images of the plasma sprayed alumina samples are shown in Figure 4 after nearly 6 years of exposure at 90°C in the salt solution described above. It can be seen that the plasma sprayed ceramic coating has blistered locally and corrosion product can be observed on top of the blisters. Interestingly, it does appear that the blistered coating remains attached to the sample probably due to bonding between the corrosion

product and the ceramic. In contrast a Detonation Gun alumina/titania coating in the same figure shows no observable outward corrosion damage. It also showed no coating damage around the slot cut in the coating.

A cross-section micrograph of a Detonation Gun coating of an alumina/titania mixture is shown in Figure 5. This particular sample had two slots cut through the ceramic coating as well as a nickel bond coat applied to the steel before the Detonation Gun coating was applied. The microstructure around the notch in the Detonation Gun coating reveals corrosion on the interior surfaces of the notch. There is also some preferential corrosion at the interface between the nickel bond coat and the steel substrate. We attribute the extra corrosion in this region to galvanic coupling between the nickel and steel. In this case the nickel is more noble than the carbon steel substrate. It can be observed that the interface between the nickel and ceramic coating remains intact and the corrosion product has not caused the overlying ceramic coating to spall off after a period of nearly 6 years at 90°C. The micrograph in Figure 5 (b) shows a region of the coating interface far away from the notch. The gray phase appears to be a corrosion product-like phase. This was the largest amount of anything that could be interpreted as a corrosion phase observed anywhere away from the notch. However, it is not clear if this phase was present on the steel prior to when the coating was applied. It appears that there is very little porosity in the coating. The Detonation Gun coatings are expected to have densities equivalent to or even denser than HVOF coatings.

## B. Corrosion Models for the Waste Package

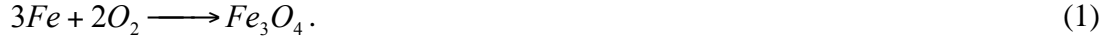
Models of idealized inorganic coatings have been developed for various environmental conditions during anticipated repository conditions [4]. During the periods of dry oxidation ( $T \geq 100^\circ\text{C}$ ) and humid-air corrosion ( $T \leq 100^\circ\text{C}$  and  $\text{RH} < 80\%$ ), it is assumed that the growth rate of oxide on the surface is diminished in proportion to the amount of surface covered by solid ceramic. During the period of aqueous phase corrosion ( $T \leq 100^\circ\text{C}$  and  $\text{RH} \geq 80\%$ ), it is assumed that the overall mass transfer resistance governing the corrosion rate is due to the combined resistances of ceramic coating and interfacial corrosion products. Modeling of only the aqueous corrosion regime is presented here. A simple porosity model (cylinder and sphere chain) is considered in estimation of the mass transfer resistance of the ceramic coating. It is evident that an impedance to  $\text{O}_2$  transport is encountered if pores are filled with liquid water. Spallation (rupture) of the ceramic coating is assumed to occur if the stress introduced by the expanding corrosion products at the ceramic-metal interface exceeds the fracture stress.

## Corrosion Reactions

The corrosion products formed on carbon steel in vapor-phase environments include goethite ( $\alpha\text{-FeOOH}$ ) and magnetite ( $\text{Fe}_3\text{O}_4$ ). In aqueous phase environments that contain chloride salts, corrosion products may also include akaganeite ( $\beta\text{-FeOOH}$ ). These products have been identified by Raman spectroscopy, and confirmed by X-ray diffraction [4]. In the case of aqueous phase corrosion, it has been shown that dissolved



oxygen is required as a cathodic reactant to promote corrosion. Since the formation of magnetite at the ceramic-metal interface would be most detrimental to the coating (based on volume change), the model developed here assumes that all corrosion product is in the form of  $Fe_3O_4$ . Oxyhydroxides such as  $FeOOH$  would probably be present as polymeric gels at the interface; however, due to the likely compliance of the gel,  $FeOOH$  was not considered in this model. The chemical reaction for the model purposes is:



#### Aqueous Phase Corrosion

Pores are completely filled with moisture in the aqueous phase corrosion model. Typical aqueous phase corrosion rates apply at the ceramic-metal interface when dripping water exists and the relative humidity (RH) is greater than 80%. It is well known that aqueous phase corrosion of carbon steel relies heavily on the cathodic reduction of oxygen for depolarization of the anodic reaction [5]. Measurements show corrosion rates increase linearly with the concentration of dissolved oxygen. The rate in completely de-aerated solution (zero concentration of dissolved oxygen) appears to be essentially zero (infinitesimally small). Therefore, the following oxygen-dependent penetration rate is assumed:

$$\frac{1}{3} \frac{\rho}{w} \frac{dp}{dt} = \frac{1}{2} k_o C \quad (2)$$

where  $C$  (in this case) is the concentration of dissolved oxygen in water contacting the carbon steel. In most cases,  $C$  is equivalent to the saturation concentration,  $C_{sat}$ . From the published data of Uhlig and Revie [5], the extrapolated penetration rate of carbon steel after 48 hours exposure at 25°C to a solution containing 165 ppm  $CaCl_2$  and 6 ml/liter dissolved  $O_2$  is approximately 93.46 mg/dm<sup>2</sup>/day. The apparent rate constant,  $k_o$ , can be calculated from the slope of this plotted data, which is 15.576 mg/dm<sup>2</sup>/day per ml/liter.

The following equation provides the concentration of dissolved oxygen in the water contacting the carbon steel as a function of temperature and salt concentration [6].

$$\ln(C_{sat}) = A_1 + A_2 \left( \frac{100}{T} \right) + A_3 \ln \left( \frac{T}{100} \right) + A_4 \left( \frac{T}{100} \right) + S \left[ B_1 + B_2 \left( \frac{T}{100} \right) + B_3 \left( \frac{T}{100} \right)^2 \right] \quad (3)$$

In this equation,  $C_{sat}$  is the saturation concentration of dissolved oxygen in water (ml  $O_2$  per liter  $H_2O$ ),  $T$  is the absolute temperature (K), and  $S$  is the total concentration of dissolved salt (parts per thousand). The coefficients  $A_i$  and  $B_i$  are defined in Table III below.

Table III. Coefficients for the Calculation of Dissolved Oxygen in Salt-Containing Water

Coefficient	i = 1	i = 2	i = 3	i = 4
A <sub>i</sub>	-173.4292	249.6330	143.3483	-21.033096
B <sub>i</sub>	-0.033096	0.014259	-0.0017000	

Conversion of this quantity (ml O<sub>2</sub> per liter of H<sub>2</sub>O) to more conventional units is done as follows:

$$C_{sat} (mol / cm^3) = B \frac{P}{RT} C_{sat} (ml / liter) \quad (4)$$

where P is atmospheric pressure (atm), T is the absolute temperature (K), R is the universal gas constant (82.056 atm cm<sup>3</sup> mol<sup>-1</sup> K<sup>-1</sup>), and B is a conversion factor (0.001 liters per cm<sup>3</sup>).

#### Diffusive Flux through the Porous Ceramic Coating

Development of an appropriate model begins with consideration of the flux of oxygen through multiple diffusion barriers, represented by subscripts I and O (see Figure 6).

$$J = k_I (a - a_i) = k_O (a_i - a_s) = K (a - a_s) \quad (5)$$

The parameters  $k_I$  and  $k_O$  are the individual mass transfer coefficients for barriers I and O, respectively,  $K$  is the overall mass transfer coefficient for both barriers,  $a$  is the activity of the transported reactive species at the outer surface of barrier I,  $a_i$  is the activity at the interface separating barriers I and O, and  $a_s$  is the activity at the interface separating barrier O and the metal substrate. The barrier I represents the ceramic coating, the barrier O represents the accumulated interfacial corrosion product Fe<sub>3</sub>O<sub>4</sub>, the metal substrate is carbon steel, and the transported reactive species is dissolved oxygen in pore water (aqueous phase corrosion). Furthermore, it is also assumed that the chemical activity ( $a$ ) can be approximated by concentration ( $C$ ). Subscripts  $i$  and  $s$  represent the interface and carbon steel substrate respectively.

#### Physical Definition of Overall Mass Transfer Coefficient (Resistance)

The overall mass transfer coefficient (mass transfer resistance) can be expressed in terms of the individual mass transfer coefficients as described by Sherwood, Pigford and Wilke [7].

$$\frac{1}{K} = \frac{1}{k_O} + \frac{1}{k_I} \quad (6)$$

The individual mass transfer coefficients are given physical definition by introducing a simple porosity model. For example, in the case of the ceramic coating, pores are first treated as long, straight cylinders of length  $\delta$ . The flux of corroding species through such a pore is then approximated by:

$$J_{pore} = \frac{D_l}{\delta} (C - C_i) \quad (7)$$

The average flux of oxygen per unit area of waste package is then:

$$J = \frac{\theta_l D_l}{\delta} (C - C_i) \quad (8)$$

where  $D_l$  is the bulk diffusivity of the corroding species in the pore and  $\theta_l$  is the fraction of the metal exposed to the aqueous phase at the ceramic-metal interface. This can be interpreted as porosity. Values of 0.02-0.03 have been achieved with HVOF ceramic coatings having thicknesses of approximately 1.5 mm. Thus far, thicker coatings have been significantly more porous. The porosity in actual HVOF and plasma-sprayed coatings can be observed in micrographs in Figure 2. The porous interfacial corrosion product is modeled in a similar fashion:

$$J = \frac{\theta_o D_o}{x} (C_i - C_s) \quad (9)$$

where  $x$  is the thickness of the accumulated corrosion product,  $D_o$  is the effective diffusivity of the corroding species through the accumulated corrosion product and  $\theta_o$  is the effective porosity of the accumulated corrosion product. At the point when the reaction of corroding species with the metal substrate becomes entirely mass-transport limited, the concentration  $C_s$  drops to zero. Note that surface diffusion in the pores has been neglected. Assuming straight cylindrical pores, the physical definition of the overall mass transfer coefficient is then:

$$\frac{1}{K} = \frac{1}{k_0} + \frac{1}{k_l} = \frac{x}{\theta_o D_o} + \frac{\delta}{\theta_l D_l} \quad (10)$$

In reality, the pores in the ceramic coating are not as simple as portrayed in the above straight hollow cylinder visualization. Actually, the pores in ceramic coatings can be better represented by an array of chains, each link being composed of a hollow sphere and a relatively narrow hollow cylinder, connected in series. A more precise representation has been developed by Hopper [8], which has become known as the cylinder-sphere chain (CSC) porosity model. In this case, the flux (individual mass transfer coefficient) is diminished by a correction factor,  $f(\epsilon, \lambda)$ , where  $\epsilon$  and  $\lambda$  are dimensionless parameters used to further characterize the porous structure.

$$k_{I,corrected} = f(\varepsilon, \lambda) \times k_I \quad (11)$$

where  $f(\varepsilon, \lambda)$  is defined as:

$$f(\varepsilon, \lambda) = \frac{3}{2} \frac{(1 + \lambda)^2}{\lambda} \varepsilon^2 \quad (12)$$

Thus, the overall mass transfer coefficient is defined as:

$$\frac{1}{K} = \frac{x}{\theta_0 D_0} + \frac{\delta}{f(\varepsilon, \lambda) \theta_I D_I} \quad (13)$$

Here the dimensionless parameters  $\varepsilon$  and  $\lambda$  represent the geometry of the sphere-cylinder chain as illustrated in Figure 7:

$$\varepsilon = \frac{\text{diameter of cylinder in chain}}{\text{diameter of sphere in chain}} \quad (14)$$

$$\lambda = \frac{\text{length of cylinder in chain}}{\text{diameter of sphere in chain}} \quad (15)$$

Reasonable estimates for  $\varepsilon$  and  $\lambda$ , based on actual microstructures, are as follows:

$$0.01 \leq \varepsilon \leq 0.10 \quad (16)$$

$$2 \leq \lambda \leq 10 \quad (17)$$

Typical values of  $f(\varepsilon, \lambda)$  are illustrated below:

$$f(0.03, 10) = 0.016$$

$$f(0.05, 10) = 0.045$$

#### Parabolic Isothermal Growth of Interfacial Oxide with O<sub>2</sub> Reduction Alone

Formation of one (1) mole of Fe<sub>3</sub>O<sub>4</sub> requires the transport of two (2) moles of molecular oxygen and the consumption of three (3) moles of iron. Stated in a slightly different way, the molar production rate of Fe<sub>3</sub>O<sub>4</sub> is one-third (1/3) that of the molar consumption rate of iron and one-half (1/2) the molar consumption rate of molecular oxygen. Therefore, a relationship is established between the flux of corroding species through the protective ceramic coating, the penetration rate of the carbon steel (dp/dt), and the growth rate of the interfacial oxide (dx/dt):

$$\frac{\rho_o}{w_o} \frac{dx}{dt} = \frac{1}{3} \frac{\rho}{w} \frac{dp}{dt} = \frac{1}{2} J = \frac{1}{2} KC \quad (18)$$

After substitution of the expression for the overall mass transfer coefficient, this equation is rearranged to yield:

$$\frac{dx}{dt} = \frac{w_o}{\rho_o} \left\{ \left[ \frac{x}{\theta_o D_o} + \frac{\delta}{f(\varepsilon, \lambda) \theta_l D_l} \right]^{-1} \frac{C}{2} \right\} \quad (19)$$

This expression is then integrated, assuming isothermal conditions, to determine the dependence of the interfacial oxide thickness on time. However, prior to integration, the overall mass transfer coefficient must be rewritten in terms of oxide thickness:

$$\int_{x_0}^x \left[ \frac{x}{\theta_o D_o} + \frac{\delta}{f(\varepsilon, \lambda) \theta_l D_l} \right] dx = \int_{t_0}^t \frac{1}{2} \frac{w_o}{\rho_o} C dt \quad (20)$$

Integration shows that the oxide thickness and time are related by a simple quadratic equation:

$$\left[ \frac{1}{2\theta_o D_o} \right] x^2 + \left[ \frac{\delta}{f(\varepsilon, \lambda) \theta_l D_l} \right] x - \frac{1}{2} \frac{w_o}{\rho_o} C t = 0 \quad (21)$$

Solution of this simple quadratic equation yields the following relationship between oxide thickness, time and ceramic coating properties:

$$x = \left[ \left\{ \frac{\delta}{f(\varepsilon, \lambda) \theta_l D_l} \right\}^2 + (\theta_o D_o) \frac{w_o}{\rho_o} C t \right]^{1/2} - \left\{ \frac{\delta}{f(\varepsilon, \lambda) \theta_l D_l} \right\} \quad (22)$$

The thickness of the interfacial oxide increases with time. As the oxide becomes thicker, the growth rate decreases (Wagner's law). The relationship between oxide thickness and wall penetration is:

$$x = \frac{1}{3} \left( \frac{\rho}{\rho_o} \frac{w_o}{w} \right) p \quad (23)$$

**First Failure Criterion Considered – Membrane Stress in Expanded Cylindrical Membrane**

Two alternative stress models are presented to account for spallation of the ceramic coating. In the first case, the ceramic coating is treated as a cylindrical membrane having infinitesimal thickness, as shown in Figure 8. A fracture toughness criterion would likely

be more appropriate but for the results presented here a failure stress will be considered to include the effects of flaw population size in the coatings. The rate of expansion of the inner radius of the ceramic barrier coating is estimated from the interfacial displacement, which accounts for the conversion of Fe to  $\text{Fe}_3\text{O}_4$  (expansion), as well as the simultaneous loss of carbon steel (contraction).

$$\frac{dR}{dt} = \frac{d(x - p)}{dt} \quad (24)$$

The difference between the oxide thickness and the wall penetration  $(x - p)$  is defined as the interfacial displacement. The strain in the coating, around the circumference of the container, is proportional to the change in inner radius

$$\frac{de}{dt} = \frac{1}{2\pi R} 2\pi \frac{dR}{dt} \quad (25)$$

which can be written more simply as:

$$\frac{de}{dt} = \frac{1}{R} \frac{dR}{dt} \quad (26)$$

The uniaxial stress and strain are related by the elastic modulus, E:

$$\sigma = E \times e \quad (27)$$

For example, the fracture strain of a porous ceramic exposed to water can be estimated from the elastic modulus and the fracture stress as follows:

$$e^* = \frac{\sigma^*}{E} = \frac{16.7 \text{ MPa}}{356,000 \text{ MPa}} = 4.691 \times 10^{-5} \quad (28)$$

The time required for the strain to reach the fracture strain,  $\tau^*$ , determines the time to fracture. This is the time required for formation of the first crack in the ceramic coating, but does not necessarily imply complete failure of the coating.

$$\tau^* = \frac{e^*}{\int_0^t \frac{de}{dt} dt} \quad (29)$$

## Second Failure Criterion Considered - Blister Model

In this failure process it is assumed that spallation occurs at a blister, such as the one illustrated in Figure 9. To account for the formation of blisters in the ceramic coating, Roark's formulas can be used [9]. The deflection of the center of the circular

plate from the relaxed position is  $y_c$ , defined as follows:

$$y_c = -\frac{qa^4}{64D} \quad (30)$$

where  $q$  is the uniform load (pressure) exerted on the internal surface of the deflected circular plate (blister),  $a$  is the radius of the circular plate (blister), and  $D$  is the plate constant. Since the deflection is known (interfacial displacement), the uniform load can be calculated.

$$q = -\frac{64D}{a^4}y_c \quad (31)$$

The plate constant is given by:

$$D = -\frac{Et^3}{12(1-\nu^2)} \quad (32)$$

where  $E$  is the elastic modulus of the ceramic coating,  $t$  is the thickness of the plate, and  $\nu$  is Poisson's ratio. In the case of solid  $\text{Al}_2\text{O}_3$ , Adkeland gives a value of 0.26 for Poisson's ratio and a value of 379,300 MPa for the elastic modulus [10]. The bending moment at the center of the plate is  $M_c$ , defined as follows:

$$M_c = \frac{qa^4(1+\nu)}{16} \quad (33)$$

The radial moment at the fixed edge of the plate is  $M_{ra}$ , reactive, and defined as follows:

$$M_{ra} = -\frac{qa^2}{8} \quad (34)$$

The stress on the concave surface of the deflected circular plate is compressive, and the stress on the convex surface of the deflected circular plate is tensile. The tensile stress is calculated from  $M_c$  with the following formula:

$$\sigma = \frac{6M_c}{t^2} \quad (35)$$

Assuming maximum normal stress theory for a failure criterion, failure is assumed when the stress calculated from the bending moment exceeds the fracture strength of the ceramic.

## Fracture of the Protective Ceramic Coating

Growth of interfacial oxide will slowly expand the ceramic coating. This expansion or strain in the coating will induce stress. Assuming maximum normal stress theory for the failure criterion, the coating will fail at the point where the maximum stress in the ceramic coating exceeds the fracture stress. It is important to keep in mind that this failure criterion indicates fracture or a crack in the coating but does not imply that the coating has been completely removed from the substrate. The coating often appears to impart some level of continued protection in long-term corrosion tests. An order-of-magnitude estimate for fracture stresses in ceramics is used in this work. In the case of non-porous solids, the values in Table IV [11] are believed to be representative of the properties of non-porous materials.

Table IV. Representative Mechanical Properties of Ceramic Coatings

Ceramic	Elastic Modulus (E)	Elastic Modulus (E)	Fracture Strength ( $\sigma^*$ )	Fracture Strength ( $\sigma^*$ )
	MPa	Mpsi	MPa	Kpsi (or ksi)
Al <sub>2</sub> O <sub>3</sub>	365,000	53	172	25
ZrO <sub>2</sub>	144,900	21	55	8

Others have studied environmental effects on stress corrosion cracking of thermally sprayed ceramic coatings on stainless steel and titanium substrates. Specific reference is made to studies of the environmental fracture of plasma-sprayed Al<sub>2</sub>O<sub>3</sub> on metallic implants during exposures to physiological media [12]. This data is shown in Table V.

Table V. Mechanical Properties of Ceramic Coatings

Ceramic	Substrate	Environment	Fracture Strength ( $\sigma^*$ )	Fracture Strength ( $\sigma^*$ )
			MPa	Kpsi (or ksi)
Al <sub>2</sub> O <sub>3</sub>	Stainless Steel	Air, 26°C, 46% RH	17.8 ± 1.9	2.590 ± 0.273
Al <sub>2</sub> O <sub>3</sub>	Stainless Steel	Water, 25°C, Deionized	16.7 ± 1.6	2.480 ± 0.320
Al <sub>2</sub> O <sub>3</sub>	Titanium	Air, 26°C, 46% RH	17.1 ± 2.2	2.430 ± 0.230
Al <sub>2</sub> O <sub>3</sub>	Titanium	Water, 25°C, Deionized	19.1 ± 2.8	2.770 ± 0.260

Note: numbers following ± represents one standard deviation.

For the purposes of this model a lower limit for a likely fracture strength is selected from the lowest environmentally-sensitive fracture stress given in Table V (16.7 MPa). The data in Table IV might be reasonably used as a high limit for fracture strength under optimal conditions. Unfortunately, these assignments are somewhat arbitrary approximations. A summary plot indicating the stress level for membrane stress, blister failure, and possible coating strength levels is shown in Figure 10. This figure shows that with a rather conservative assumed strength for the ceramic coating materials approximately 500 years of protection against corrosion are predicted. It is interesting to note that the failure mode exhibited by the rather porous plasma sprayed alumina coatings (see Figure 4) appears to be the blister failure mode which is consistent with the model prediction (for the typical coating properties mentioned above). The results of the



model indicate higher stress in the blister failure mode as shown in Figure 10. At the high end of fracture strain for the ceramic coating, the corrosion resistance for the coating could last several thousand years. It is quite possible that this length of time would protect a waste package against corrosion during the highest temperature portion of the waste package lifetime and continue to provide protection as the radioactive decay eventually leads to lower temperatures in the waste container.

### Summary

It is evident from the experimental results that ceramic coatings with sufficiently low porosity can provide a sufficient barrier against aqueous corrosion in concentrated salt solutions at 90°C. In particular a Detonation Gun coating tested under these conditions for nearly 6 years demonstrated resistance to corrosion damage for a steel substrate even with an intentional defect (a 0.015" slot) placed in the coating. A comprehensive model including corrosion and failure criteria for the performance of the ceramic coatings in aqueous corrosion environments show that performance can be predicted based on microstructural and physical properties for the coatings. The model results suggest that with the proper microstructure and physical properties a ceramic thermal spray coating will provide significant corrosion protection lifetimes.

This work was performed under the auspices of the U.S. Department of Energy by the University of California, Lawrence Livermore National Laboratory under Contract No. W-7405-Eng-48.

## List of Figure Captions

Figure 1. Schematic illustration of (a) Plasma and (b) HVOF thermal spray gun designs.

Figure 2. Microstructure and impedance resistance measurements for HVOF coated alumina/titania and plasma sprayed alumina. The large arrow indicates the thermal spray direction.

Figure 3. Microstructures of long-term test samples after 6 months in 10X concentrated well water solution at 90°C. HVOF thermal spray coating (top) and plasma spray coating (bottom) are shown.

Figure 4. This figure shows macroscopic images of (a) ceramic coated steel samples in racks as situated in corrosion tanks, (b) close up of plasma sprayed alumina sample on left and Detonation Gun Alumina/Titania sample on right after nearly 6 years in 90°C salt solution. The waterline is approximately half way up the sample. The blistering in the plasma sprayed alumina coating is attributed to the high porosity in the coating, which allows for rapid corrosion under the ceramic coating. The discoloration on the Detonation Gun coating was from salts in the water solution, which have adsorbed onto the surface. Underneath the surface contaminates the coating appears to have the original color. A metallographic cross-section mounted sample (inset) was taken from below the water line. The arrow indicates the approximate cross-section location. The ceramic coating is a black layer of uniform thickness. No corrosion is observable below the

coating in this metallographic image. An intentional notch is located at the top of the metallographic image.

Figure 5. This micrograph shows the Detonation Gun coating of Alumina/Titania mixture on top of a nickel bond coat. The substrate is plain carbon steel. (a) The slot was cut in the coating prior to placing it in a 90°C corrosion tank. This micrograph is from a slot that was immersed in the aqueous solution for nearly 6 years. (b) This micrograph is from a region far away from the slot. The gray phase is believed to be an iron oxide and was the largest “corrosion-like” phase observed at the interface away from the slot. It is not certain whether the oxide was already present on the steel prior to the application of the coating. The large black lamellar particles in the coating are believed to be solid; no large pores are easily observed.

Figure 6. This is an illustration of parameters associated with diffusion of oxygen through inorganic coating. Subscript,  $I$ , is associated with the ceramic coating and subscript,  $O$ , is associated with the iron oxide corrosion product.

Figure 7. This is an illustration of idealized porosity used to model pore structure in inorganic thermal spray coatings which is called the Cylinder-Sphere Chain (CSC) porosity model [8].

Figure 8. This figure illustrates the model of stress in an expanded cylinder. The subscripts are the same as in Figure 6.

Figure 9. This is an illustration of the blister model for failure of ceramic coating due to localized growth of oxide underneath the ceramic coating. The load applied to the coating due to the oxide growth is  $q$ , and the radius of the blister is  $a$ .

Figure 10. This plot shows stress predicted in the coating due to blister and membrane stress failure mechanisms. A range of possible strengths of ceramic coatings (as described in the text) is indicated. For the calculation of membrane stress the diameter of the substrate was 1 meter.

## Figures

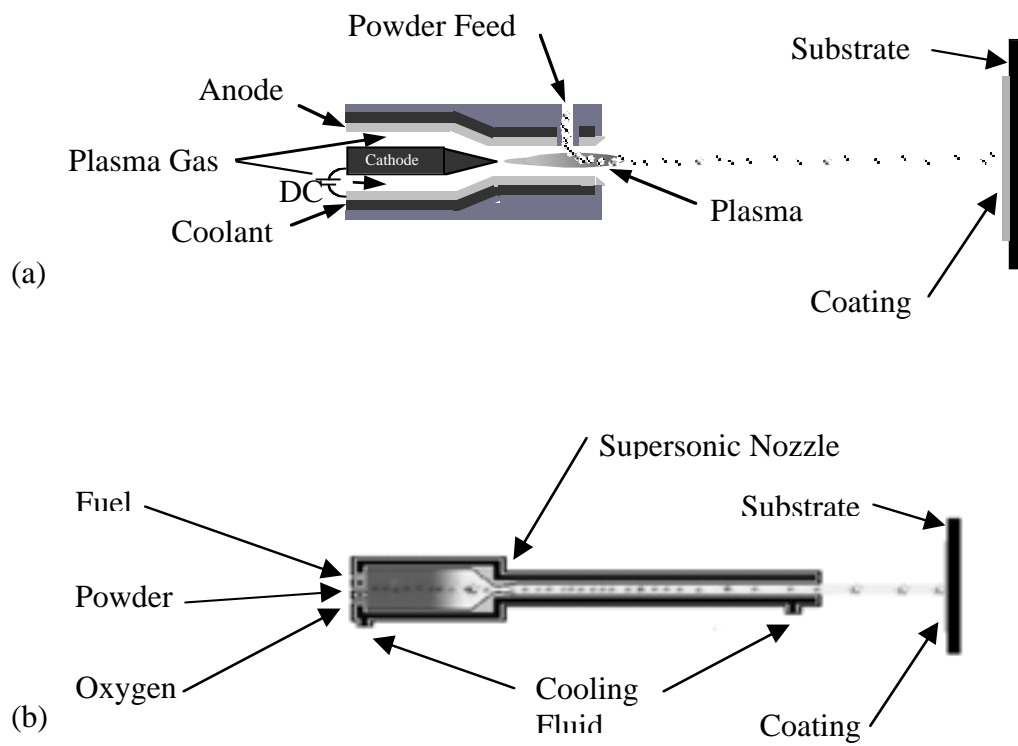


Figure 1. Schematic illustration of (a) Plasma and (b) HVOF thermal spray gun designs.

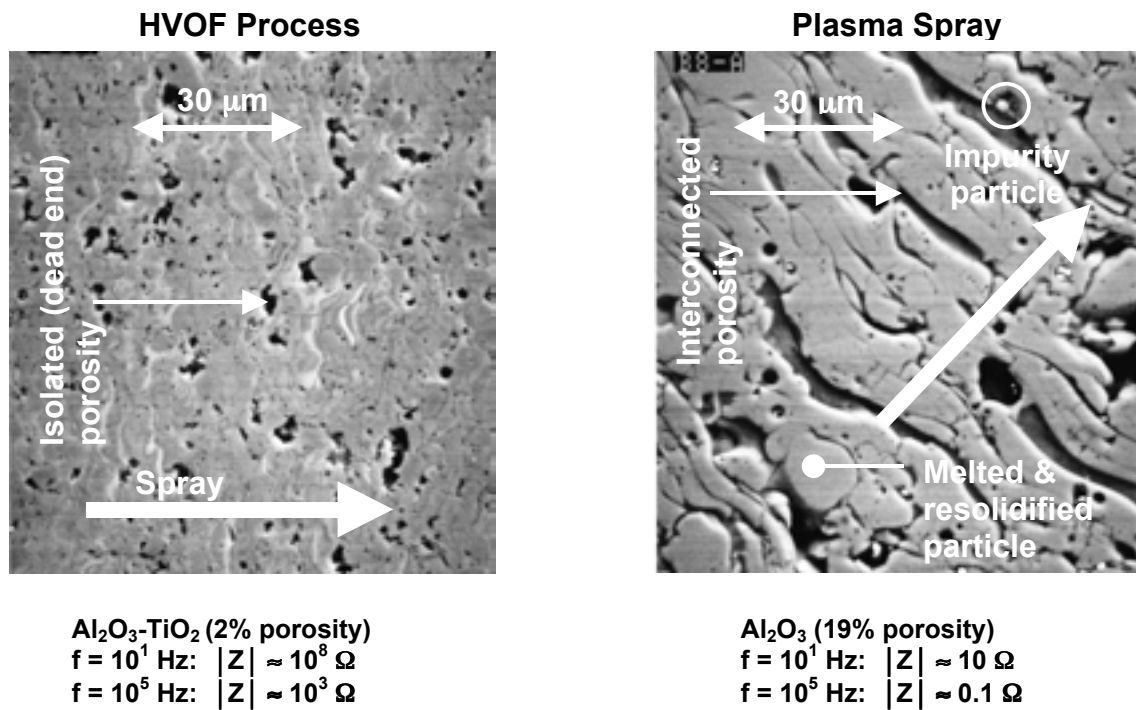


Figure 2. Microstructure and impedance resistance measurements for HVOF coated alumina/titania and plasma sprayed alumina. The large arrow indicates the thermal spray direction.

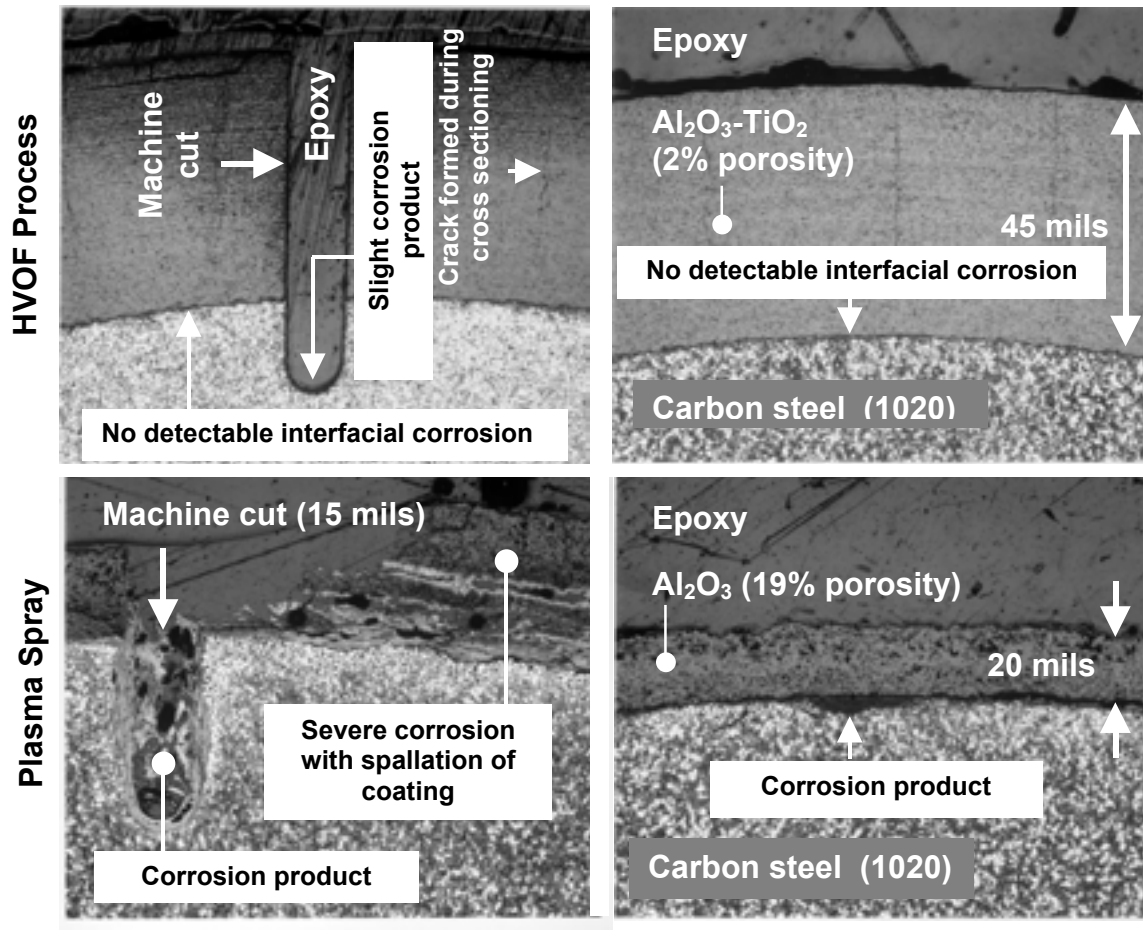


Figure 3. Microstructures of long-term test samples after 6 months in 10X concentrated well water solution at 90°C. HVOF thermal spray coating (top) and plasma spray coating (bottom) are shown.

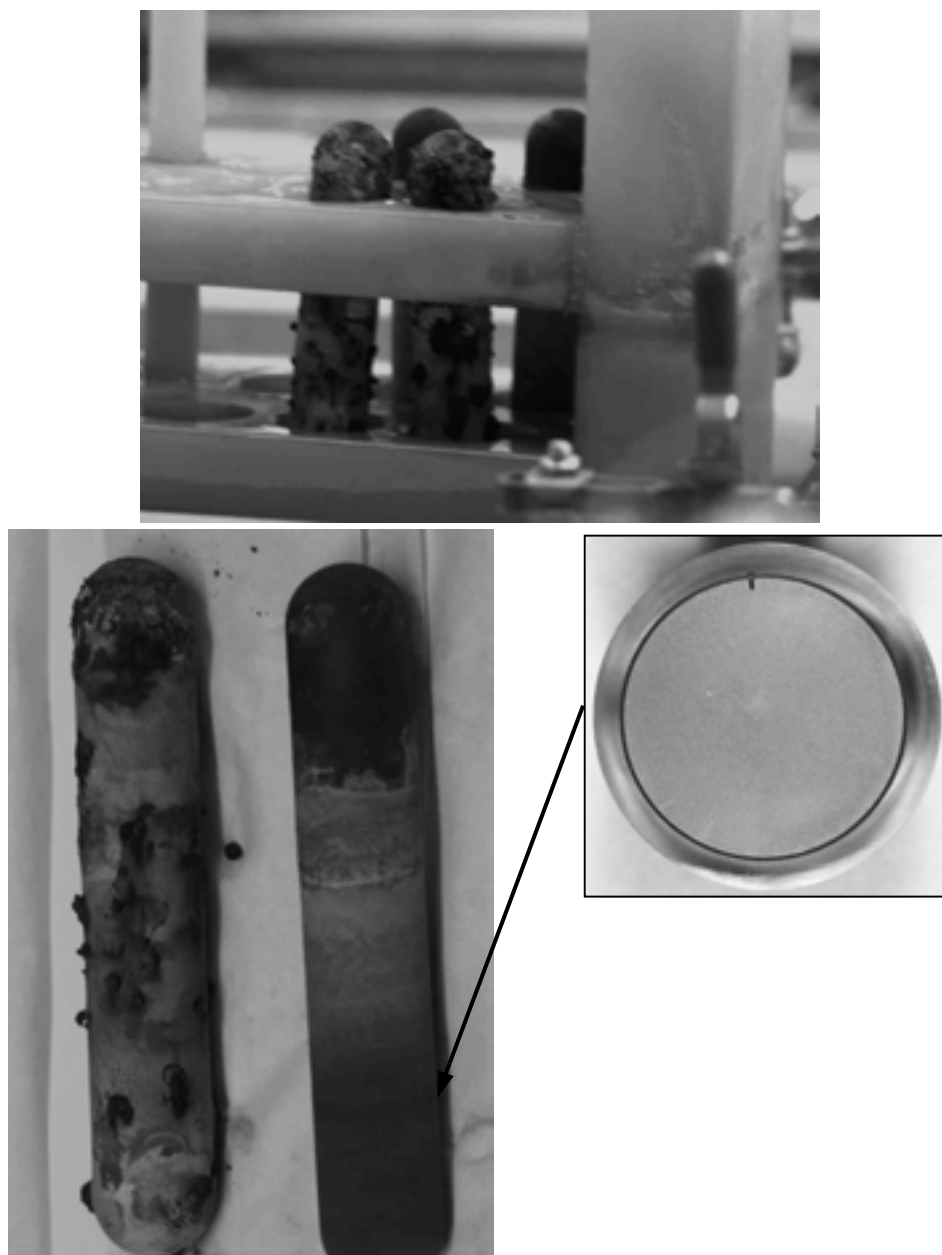


Figure 4. This figure shows macroscopic images of (a) ceramic coated steel samples in racks as situated in corrosion tanks, (b) close up of plasma sprayed alumina sample on left and Detonation Gun Alumina/Titania sample on right after nearly 6 years in 90°C salt solution. The waterline is approximately half way up the sample. The blistering in the plasma sprayed alumina coating is attributed to the high porosity in the coating, which allows for rapid corrosion under the ceramic coating. The discoloration on the Detonation Gun coating was from salts in the water solution, which have adsorbed onto the surface. Underneath the surface contaminates the coating appears to have the original color. A metallographic cross-section mounted sample (inset) was taken from below the water line. The arrow indicates the approximate cross-section location. The ceramic coating is a black layer of uniform thickness. No corrosion is observable below the coating in this metallographic image. An intentional notch is located at the top of the metallographic image.



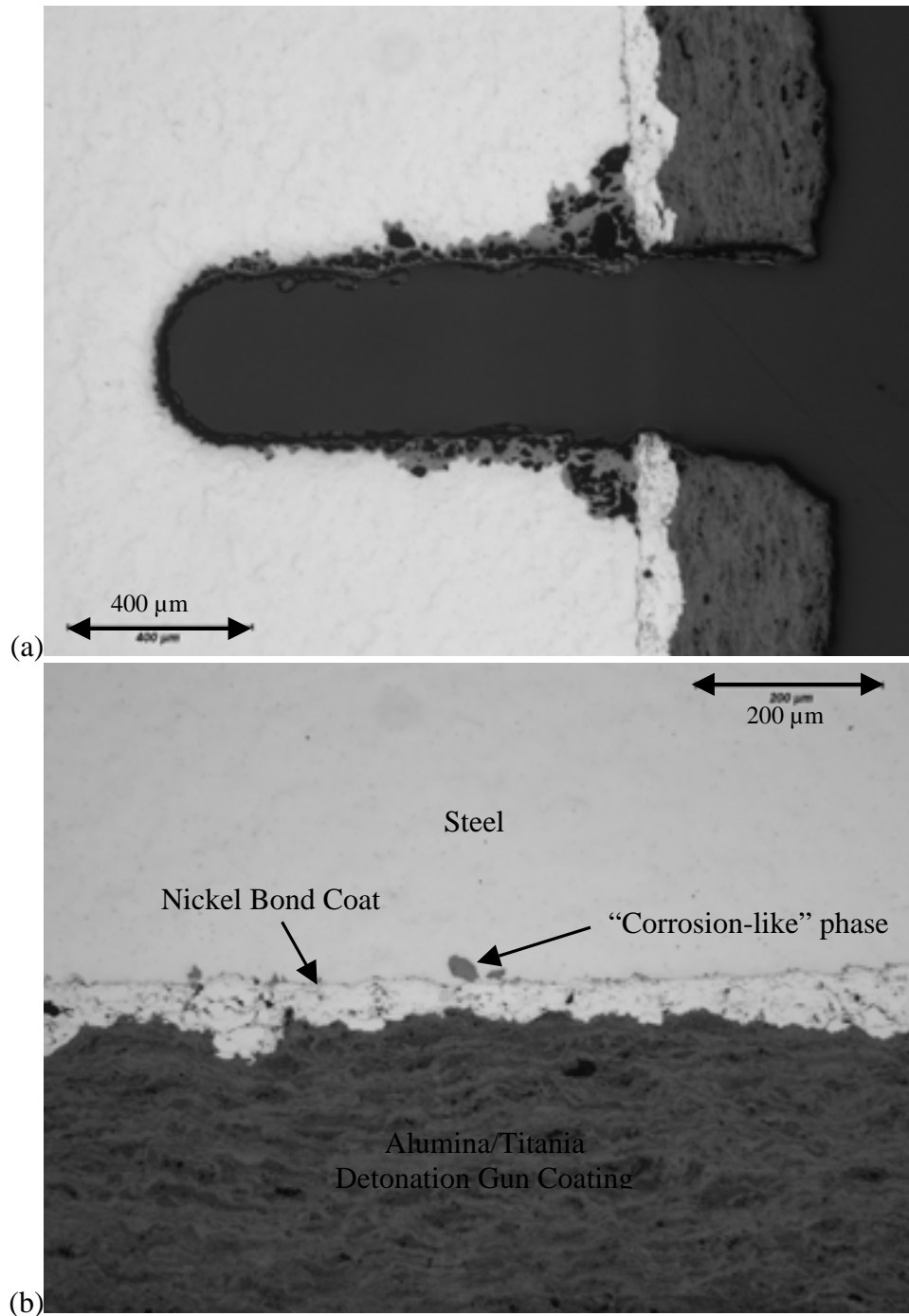


Figure 5. This micrograph shows the Detonation Gun coating of Alumina/Titania mixture on top of a nickel bond coat. The substrate is plain carbon steel. (a) The slot was cut in the coating prior to placing it in a 90°C corrosion tank. This micrograph is from a slot that was immersed in the aqueous solution for nearly 6 years. (b) This micrograph is from a region far away from the slot. The gray phase is believed to be an iron oxide and was the largest “corrosion-like” phase observed at the interface away from the slot. It is not certain whether the oxide was already present on the steel prior to the application of the coating. The large black lamellar particles in the coating are believed to be solid; no large pores are easily observed.

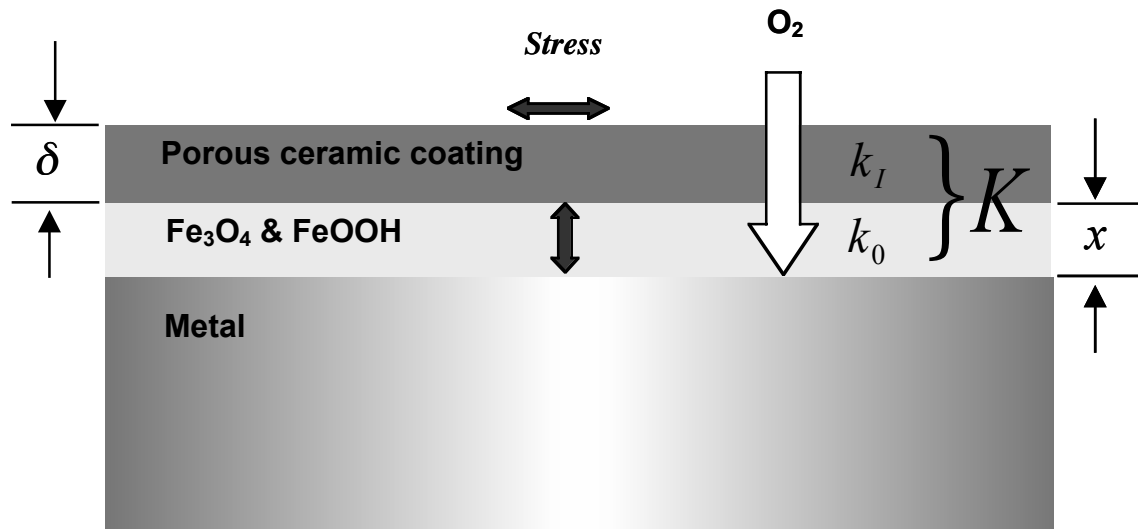
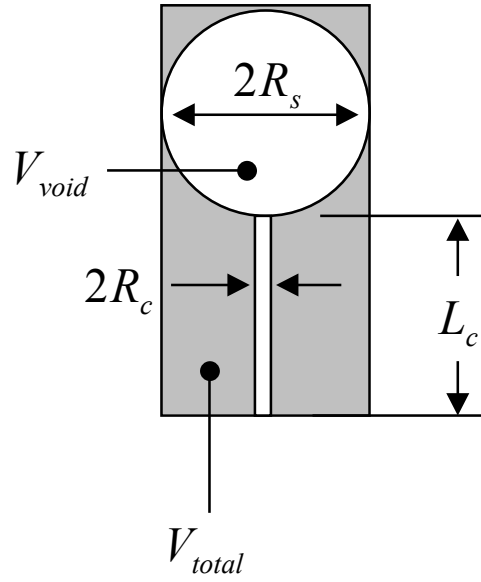


Figure 6. This is an illustration of parameters associated with diffusion of oxygen through inorganic coating. Subscript,  $I$ , is associated with the ceramic coating and subscript,  $0$ , is associated with the iron oxide corrosion product.



$$\varepsilon = \frac{2R_c}{2R_s}$$

$$\lambda = \frac{L_c}{2R_s}$$

Figure 7. This is an illustration of idealized porosity used to model pore structure in inorganic thermal spray coatings which is called the Cylinder-Sphere Chain (CSC) porosity model [8].

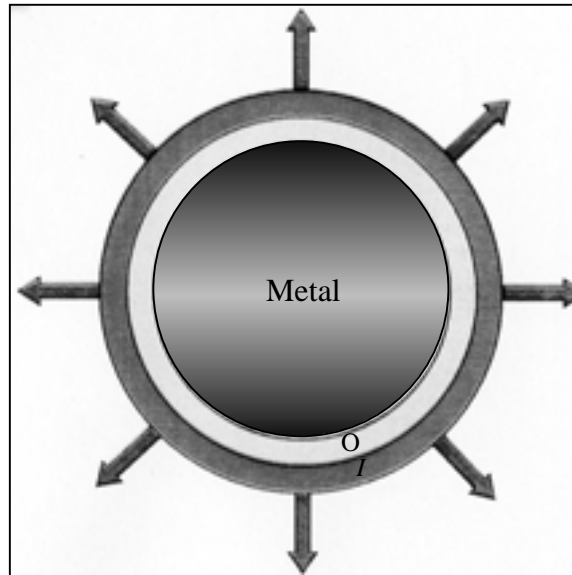


Figure 8. This figure illustrates the model of stress in an expanded cylinder. The subscripts are the same as in Figure 6.

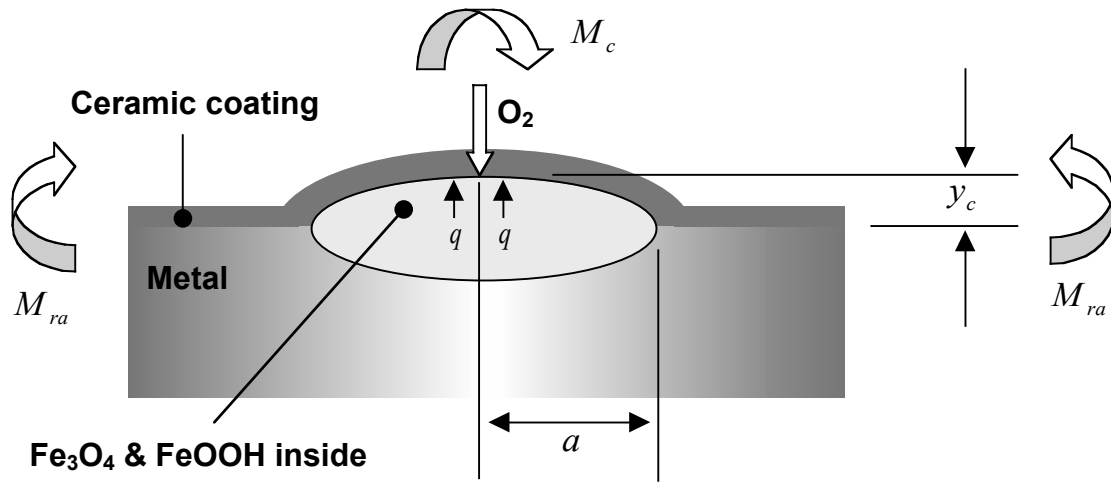


Figure 9. This is an illustration of the blister model for failure of ceramic coating due to localized growth of oxide underneath the ceramic coating. The load applied to the coating due to the oxide growth is  $q$ , and the radius of the blister is  $a$ .

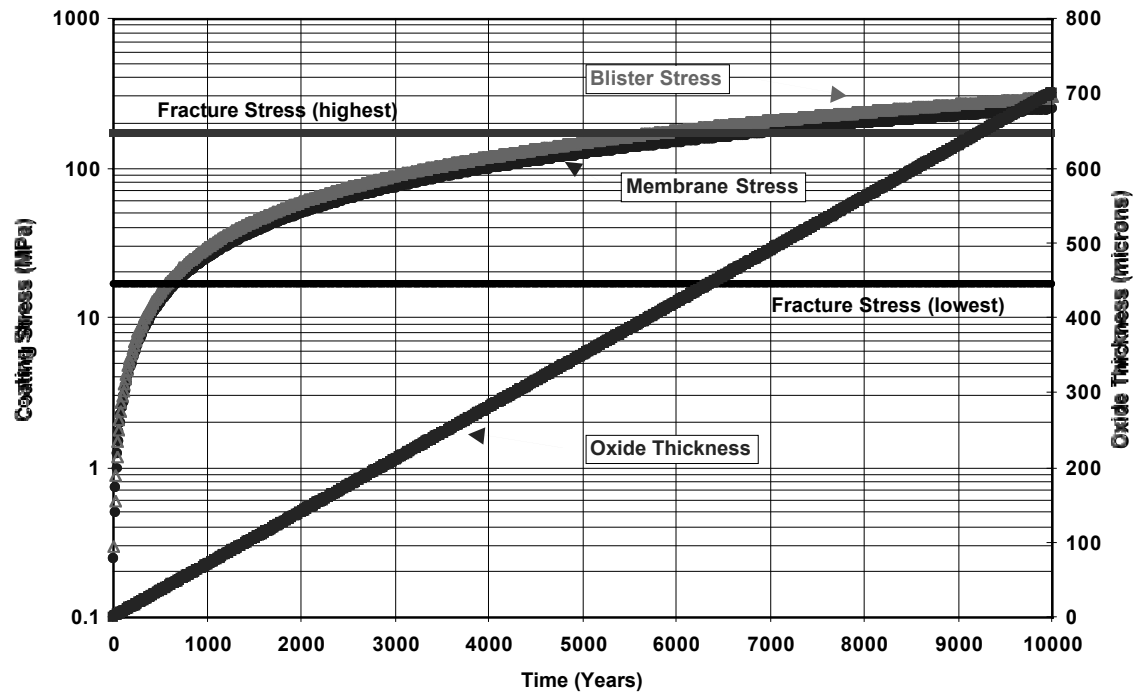


Figure 10. This plot shows stress predicted in the coating due to blister and membrane stress failure mechanisms. A range of possible strengths for the ceramic coatings (as described in the text) is indicated. For the calculation of membrane stress the diameter of the substrate was 1 meter.

## 7 References

- [1] R. D. McCright: MRS Bull., 1994, December, pp. 39-42.
- [2] R. C. Tucker, Jr.: Advanced Thermal Spray Deposition Techniques in Handbook of Deposition Technologies for Films and Coatings / Science, Technology and Applications, 2nd Edition, Edited by Rointan F. Bunshah, Noyes Publications, Park Ridge, NJ, 1994, p. 647.
- [3] A. Kulkarni, A. Vaidya, A. Goland, S. Sampath, and H. Herman: Matrls. Eng. A, 2003, vol. A359, pp. 100-111.
- [4] J. Farmer and K. Wilfinger: Internal Report, UCRL-ID-131899 Rev. 1, Lawrence Livermore National Laboratory, Livermore, CA, September 1998.
- [5] H.H. Uhlig, R. W. Revie: Corrosion and Corrosion Control, 3<sup>rd</sup> Edition, Wiley Interscience, New York, NY, 1985, p. 108; Corrosion in the Petrochemical Industry, L. Garverick, Editor, ASM International, 1994, p. 450.
- [6] D. R. Kester: Dissolved Gases Other Than CO<sub>2</sub>, Chemical Oceanography, Vol. 1, 2<sup>nd</sup> Ed, J. P. Riley, G. Skirrow, Editors, Academic Press, 1973, p. 498; Metals Handbook, Vol. 13, ASM, CD ROM Version, 1998.
- [7] T.K. Sherwood, R.L. Pigford and C.R. Wilke: Mass Transfer, McGraw-Hill, San Francisco, CA, 1975, pp. 25-26.
- [8] R.W. Hopper: Ceramic Barrier Performance Model, Version 1.0, Lawrence Livermore National Laboratory, Livermore, CA, March 1998.
- [9] W. C. Young: Roark's Formulas for Stress and Strain, 6<sup>th</sup> Ed., McGraw-Hill, San Francisco, CA, 1989, p. 429.

- [10] D. R. Adkeland, The Science and Engineering of Materials, 3<sup>rd</sup> Ed., PWS Publishing, Boston, MA, 1994, p. 141.
- [11] P.A. Thornton, V. J. Colangelo, Fundamentals of Engineering Materials, Prentice Hall, Englewood Cliffs, NJ, 07632, 1985.
- [12] M. K. Ferber and S. D. Brown: Adhesive/Cohesive Fracture Characteristics of Plasma-Sprayed Alumina Coatings Applied To 316L Stainless Steel and Ti-6Al-4V ELI Alloy Substrates in Various Physiological Media, in Fracture Mechanics of Ceramics, Vol. 6, Measurements, Transformations, and High-Temperature Fracture, R. C. Bradt, A. G. Evans, D. P. H. Hasselman, F. F. Lange, Plenum Press, New York, NY, 1983, pp. 523-544.